Materiales de Construcción
Vol. 73, Issue 350, April-June 2023, e310
ISSN-L: 0465-2746
https://doi.org/10.3989/mc.2023.298122

Development of magnesium/calcium oxalate cements

B.A. Bilginer ✉, S.T. Erdoğan

Dept. of Civil Engineering, Middle East Technical University (METU), (Ankara, Turkey)
✉: aykutb@metu.edu.tr

Received 19 July 2022
Accepted 18 January 2023
Available on line 11 April 2023

ABSTRACT: Magnesium oxalate cement, a novel alternative to portland cement, can be made at room temperature by reacting dead-burned magnesia and salts of oxalic acid. Since oxalic acid can be made using captured carbon dioxide, oxalate cements may even be carbon negative. However, emissions related with the decarbonation of magnesite at high temperatures make this hard to achieve. This study investigates the effect of replacing magnesia with granulated blast furnace slag on some physical and mechanical properties, as well as the mineralogy and microstructure of oxalate cements. Whewellite and Weddellite are identified when slag is used, in addition to Glushinskite which forms from magnesia. Slag-only mortars undergo faster but less complete reactions and show lower resistance to water than their magnesium oxalate counterparts. An equal-part combination of dead-burned magnesia and slag gives the highest 28-d strength (> 35 MPa), pH~7, and high water resistance.

KEY WORDS: Cement; Oxalate; Slag; Magnesia; Carbon dioxide.

Citation/Citar como: Bilginer, B.A.; Erdoğan, S.T. (2023) Development of magnesium/calcium oxalate cements. Mater. Construcc. 73 [350], e310. https://doi.org/10.3989/mc.2023.298122.

RESUMEN: *Desarrollo de cementos de oxalato de magnesio/calcio.* El cemento de oxalato de magnesio, una alternativa novedosa al cemento portland, puede fabricarse a temperatura ambiente haciendo reaccionar magnesia calcinada y sales de ácido oxálico. Dado que el ácido oxálico se puede fabricar utilizando dióxido de carbono capturado, los cementos de oxalato pueden incluso tener una huella de carbono negativa. Sin embargo, las emisiones relacionadas con la descarbonatación de la magnesita a altas temperaturas dificultan su consecución. Este estudio investiga el efecto de reemplazar la magnesia con escoria granulada de alto horno en algunas propiedades físicas y mecánicas, así como en la mineralogía y la microestructura de los cementos de oxalato. Whewellite y Weddellite se identifican cuando se utiliza escoria, además de Glushinskite que se forma a partir de magnesia. Los morteros solo con escoria experimentan reacciones más rápidas, pero menos completas y muestran una menor resistencia al agua que los correspondientes de oxalato de magnesio. Una combinación a partes iguales de magnesia calcinada y escoria proporciona la mayor resistencia a 28 días (> 35 MPa), pH~7 y alta resistencia al agua.

PALABRAS CLAVE: Cemento; Oxalato; Escoria; Magnesio; Dióxido de carbono.

1. INTRODUCTION

Portland cement (PC), the ubiquitous construction binder, has a considerable environmental impact. Despite its many excellent technical properties (1), its high carbon footprint and embodied energy have led to an ongoing search for lower-environmental-impact alternative binders (2-10). Many of these systems are low-carbon in comparison to PC but not carbon-neutral or negative, or require higher-than-room temperature curing, or sequester carbon into a prefabricated block, limiting versatility (11-14). A carbon-neutral/negative yet practical binder needs to use a low-cost, powder with a low carbon footprint, to be able to trap large amounts of CO_2, to be cast on site, and yield a reaction product with sufficient physical and mechanical properties. Recent studies (15-18) have proposed magnesium oxalate cement (MgOx) as a new alternative to PC. MgOx is an acid-base cement, similar to the well-known magnesium phosphate cements (MPC) (19-22). MPCs are made by reacting salts of phosphoric acid, like KH_2PO_4, with dead-burned MgO, and possess useful properties such as rapid setting, high early and ultimate strength, the ability to set and harden at very low temperatures, low shrinkage, high abrasion resistance, etc. (23). The acid-base neutralization results in a paste with near-neutral pH. These properties lend MPCs to diverse fields like biomaterials, toxic waste stabilization, and concrete repair (24-26). MgOx relies on acid-base reactions between oxalic acid salts and dead-burned MgO. Oxalic acid ($C_2H_2O_4$) is a multi-carbon chemical that is relatively easy to obtain from captured CO_2 (27-33). Schuler et al. (34) compared many methods to produce oxalic acid ($H_2C_2O_4$) or oxalate ($C_2O_4^{2-}$). Over ten of these methods started with CO_2 and were assessed, using green chemistry principles, as being among the most sustainable paths to oxalic acid. The "CO_2 equivalent"/cation is 2/1 (molar) in Ca- and Mg-oxalates. This is higher than the 1/1 ratio in Ca/Mg carbonates allowing greater amounts of CO_2 to be bound, and a low-carbon cement to be achieved. Ca- and Mg- oxalates also show low solubility in water (35). Calcium phosphate cements are widely reported, mainly as biomaterials. The precipitation of calcium oxalate crystals (CaOx) has been studied widely as they form the most prevalent type of kidney stones (36). CaOx precipitation can also be used for water proofing portland cement concrete by forming a thin surface film or by filling pores (37, 38). However, there are no accounts of calcium oxalate cements. Ca analogues of MgOx, such as those made with hydrated lime as the basic powder, can also set and harden, but high water demand and dimensional stability issues lead to high porosity and low strength. MgOx are rapid setting, can reach medium-to-high ultimate strength, and are water-resistant (15). However, like MPCs, they use dead-burned MgO. Since low-cost MgO is typically obtained by decarbonating $MgCO_3$ and burning MgO at ~1500 °C leads to significant fuel-related emissions, MgOx cements can be made low carbon but not carbon negative (15). Replacement of dead-burned MgO with a less carbon-intense waste or natural material is needed to further decrease the carbon footprint of oxalate cements. Luo et al. (39) recently reported a ferrous oxalate cement paste made with copper slag and oxalic acid. Medium to high compressive strengths were measured on 2 cm cube paste specimens but water resistance or reaction temperatures of the pastes were not reported. Various studies on MPCs have found that dead burned MgO can be replaced with up to 50 % industrial byproducts such blast furnace slag, steel slag, red mud, or fly ash, without negative effects on mechanical properties and/or water resistance (40-43). This study attempts to partially or fully replace dead-burned MgO with ground granulated blast furnace slag, as an alkaline powder with a low carbon footprint and low cost.

2. MATERIALS AND METHODS

2.1. Materials

Low-grade magnesia (MgO) was purchased in powder form. As this powder dissolves too quickly in an acidic solution, it was calcined for 1 h at 1500 °C to obtain dead-burned magnesia (MgO1500) (44). After calcination, the hard mass obtained was ground to a powder. Ground granulated blast furnace slag (GGBFS) was received, in powder form, from Kardemir Iron and Steel Plant in Karabük, Turkey. The magnesia and slag were used as the alkaline component of the acid-base mixtures. The fly ash (FA) used was received from Afşin-Elbistan Thermal Power Plant in Turkey. Technical grade oxalic acid dihydrate (OxAc) was received from Balmumcu Chemical Industries in Ankara, Turkey. Reagent grade borax, $Na_2B_4O_7 \cdot 10H_2O$ (Merck), was also used, as a set retarder. The oxide compositions of the main ingredients (MgO, MgO1500, FA, and GGBFS) determined using X-ray fluorescence spectrometry (XRF, Rigaku ZSX Primus), are provided in Table 1.

As expected, calcination does not greatly affect the oxide composition of the magnesia but mainly decreases the measured CO_2 content. Loss on ignition measurements parallel this loss upon calcination. Nevertheless, MgO1500 still contains some CO_2. This could be due to some organic impurities in the as-received magnesia forming carbon upon calcination or due to problems with detecting/measuring the lightweight (and low x-ray fluorescence yield) element carbon with semi-quantitative XRF.

The fly ash is "high-lime" as per ASTM C 618 (45) with ~21 % CaO and > 50 % SiO_2+Fe_2O_3+Al_2O_3.

TABLE 1. Oxide composition and density of the main ingredients.

Oxide	Mass (%)			
	MgO	MgO1500	FA	GGBFS
MgO	81.30	82.80	2.26	5.90
SiO_2	9.35	10.60	40.09	39.70
CaO	1.74	1.85	21.24	36.90
Al_2O_3	0.06	0.08	16.24	10.50
Fe_2O_3	0.60	0.72	7.21	1.10
CO_2	6.89	3.82	-	-
NiO	0.12	0.13	-	-
SO_3	-	-	6.71	1.20
TiO_2	-	-	0.77	0.68
P_2O_5	-	-	0.40	0.01
K_2O	-	-	1.33	0.78
MnO	-	-	-	2.20
Density (g/cm³)	3.10	3.40	2.00	3.00
Loss on ignition (%)	8.0	0	4.0	0.5
Blaine Fineness (cm²/g)	10000	2000	3300	4100

More than 3 million tons/year of this ash are produced, and its high SO_3 content makes it unsuitable for use as a pozzolan in PC systems. The slag is "hydraulically active" with (CaO + MgO) / SiO_2 > 1.0, as per EN 197-1 (46). The fly ash was used to produce a low-cost intermediate oxalic acid salt (FAOx), analogous to KH_2PO_4 used in magnesium phosphate cements. It was used to provide oxalate ions to the system in a controlled fashion. Figure 1 summarizes the production method for FAOx.

FA:OxAc:water are mixed at 1.0:1.5:1.0 by mass as in (15). The resulting paste heats up and within minutes sets into a strong but water-soluble solid. The paste is oven-dried at 105 °C for 24 h, crushed, and then ground for 45 min in a laboratory ball mill to obtain a powder. The specific gravity of FAOx was measured as 1.96. Figure 2 shows the mineralogies of the raw materials and FAOx, determined using x-ray powder diffraction (XRD). Periclase is the main phase in MgO1500 with major peaks at ~42.5 and ~37 °2θ. Forsterite (Mg_2SiO_4) is formed by the solid-state reaction of MgO and SiO_2 at high temperatures (47). FAOx shows peaks for whewellite (~24 °2θ) and quartz (~27 °2θ). Whewellite ($CaC_2O_4 \cdot H_2O$) is a calcium oxalate formed by calcium in the FA used and oxalic acid. Quartz carries from the fly ash itself. The slag is amorphous, with a characteristic hump around ~30 °2θ.

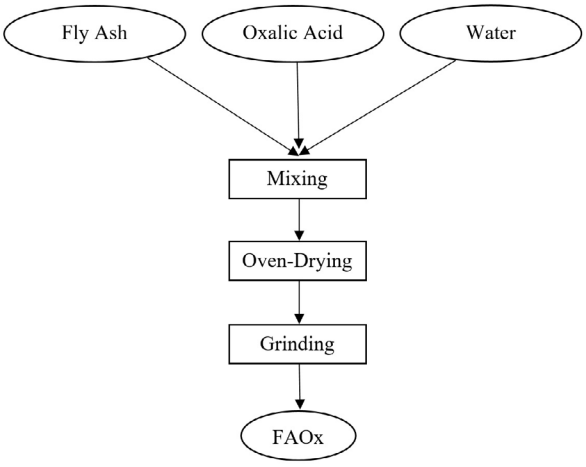

FIGURE 1. The production of FAOx.

The particle size distributions for MgO1500, slag, and FAOx were measured using laser diffraction (Malvern Mastersizer 2000) on dry powders (Figure 3). All three powders have median particle sizes 10-20 μm.

2.2. Methods

The mixture proportions given in Table 2 were used to prepare mortar and paste (same proportions but without sand) samples for various characterization tests.

The mixture proportions in Table 2 were chosen to achieve a low estimated carbon footprint and adequate mechanical performance. The FAOx-to-alkaline binder ratio influences the strength and water resistance of oxalate binders and a ratio close to 2 is close to optimum when MgO1500 is used (15). The calcination of $MgCO_3$ to produce 1 g MgO emits ~1.1 g chemical CO_2. Assuming 0.4 g fuel-related

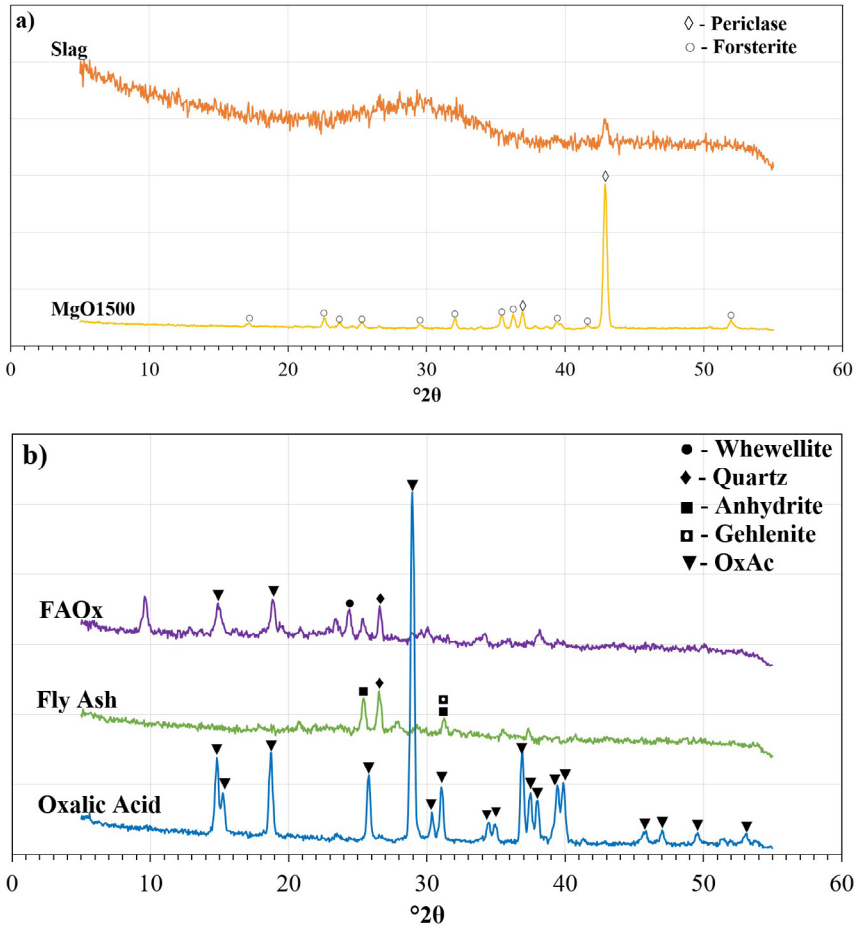

Figure 2. X-ray diffractograms of: a) the alkaline materials; b) the acid salt FAOx and the raw materials used to produce it.

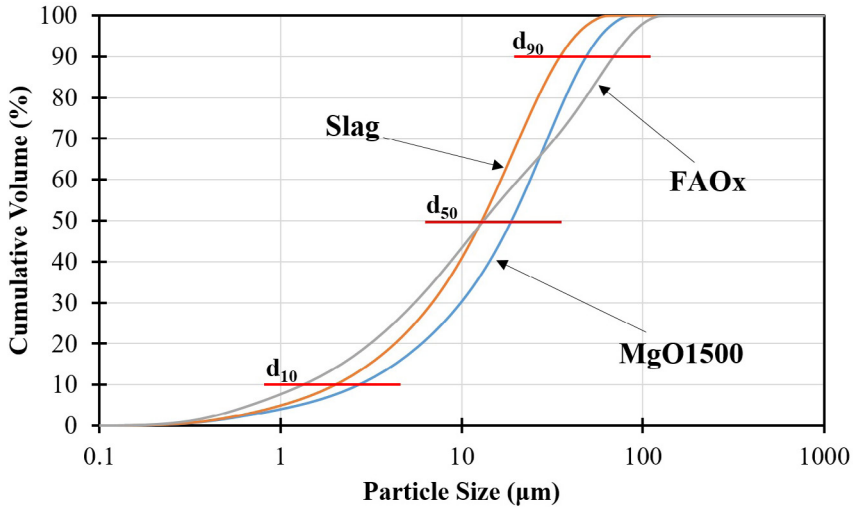

Figure 3. Particle size distributions of the powders used.

Table 2. Mixture proportions used to prepare mortar samples.

Mixture	FAOx	MgO1500	Slag	Borax*	Sand	Water
MgOx-6/4	6	4	-	0.5	20	3
MgOx-7/3	7	3	-	0.5	20	3
SlOx-6/4	6	-	4	1	20	3
SlOx-7/3	7	-	3	1	20	3
MgSlOx	7	1.5	1.5	0.5	20	3

*i.e. 10 % of binder (FAOx+Slag) mass for SlOx

CO_2 is released to obtain dead-burned MgO (at a temperature similar to PC clinker production) (48), the total emitted CO_2 becomes ~1.5 g per 1 g of MgO1500. FAOx (1 part FA and 1.5 parts OxAc) has FA:$C_2O_4^{2-}$ ~1.0, which means half of the FAOx mass is equivalent CO_2. Hence, carbon neutrality/negativity can be achieved only when FAOx:MgO1500 ≥ 3.0. Slag has a chemical carbon footprint of zero but operations like grinding make it slightly positive. Hence the two SlOx mixtures and the MgSlOx mixture in Table 2 may be carbon-negative but the two MgOx mixtures are not. Acid-base mixtures exhibit different behavior than portland cement pastes in the fresh state. Their stronger shear-thinning character and their short setting times do not provide a long time period over which flow is constant (especially for SlOx mixtures). The water-to-binder ratio (W/B) of 0.30 chosen for all mixtures is roughly the lowest value that allows adequate mixing and compaction of fresh mortars. The sand-to-binder ratio was chosen as 2.0 to give a paste/aggregate ratio similar to that in standard PC mortars. 5 % borax was used in MgOx to sufficiently retard setting. SlOx mixtures react more rapidly than MgOx, so a higher amount of borax was needed.

2.2.1. Compressive strength development

50-mm mortar cubes were tested as in ASTM C109 (49), but sample preparation slightly differed in that the mixture was mixed by hand in batches of ~300 cm^3. FAOx was first mixed with water to obtain a paste to which sand was added, followed by further mixing and the addition of the alkaline powder (MgO1500 or slag). The samples were demolded after 1 h, cured at ~24 °C and ~35 % RH, and tested at 4 h, 1 d, 7 d, and 28 d using a 250 kN Universal Testing Machine, at a loading rate of 1.5 kN/s.

2.2.2. Investigation of mineralogy and microstructure

XRD analysis (BTX II, Olympus, Japan) was performed between 5 and 55 °2θ, with a resolution of 0.25 °2θ, on < 150 μm powders obtained from reacted pastes at 1, 7, and 28 d to investigate mineralogical changes due to reactions. Cu Kα radiation was selected with a current of 330 μA and a tube voltage of 30 kV. The nature and quantity of solid phases in the reacted pastes were also investigated using thermogravimetric analysis, TGA (SDT 650, TA Instruments, USA), for paste samples air-cured for 1 d and 35 d by heating in a N_2 environment to 900 °C at 20 °C/min. The microstructures of the reacted pastes were studied with scanning electron microscopy, SEM (Quanta 400F, FEI Philips, USA), on 35-d-old samples.

2.2.3. Change in pH

The pH of paste samples was measured, initially on the fresh paste (time ~zero) and subsequently on hardened samples at 1 h, 24 h, and 7 d, with a pH meter (pH/CON 300, Oakton Instruments, USA). The fresh pastes were diluted by adding an equal mass of distilled water to obtain a more repeatable reading. Hardened samples were ground with a mortar and pestle, and pH was measured on suspensions of 10 g of ground paste and 10 g of distilled water (50).

2.2.4 Mercury Intrusion Porosimetry (MIP)

Mercury intrusion porosimetry, MIP (Poremaster 60, Quantachrome Instruments, USA) was used to analyze the pore size distribution of paste samples, cured at ~24 °C and ~35 % RH for 25 d. The maximum pressure was selected as 345 MPa. The contact angle and surface tension of mercury were assumed to be 140 ° and $480x10^{-3}$ N/m.

2.2.5. Temperature change

The change in the temperature of the mixtures due to ongoing reaction was recorded using a semi-adiabatic setup (51). Extruded polystyrene containers with lids (with an opening to introduce materials and another for a thermocouple) were used. W/B was chosen as 0.45 to ensure adequate mixing. The recording was started, and FAOx and borax were sub-

sequently added to the water, and the mix was stirred for 60 s. The alkaline powder was then introduced, the obtained paste stirred for another 60 s. The opening was shut, and temperature was measured up to 30 min. The effect on temperature of introducing the alkaline powder at different times (0, 1, 5, or 10 minutes) after mixing FAOx and water was also investigated.

2.2.6. Water resistance

The water resistance of the mortars was evaluated by determining the retained strength (%) after water submersion. The 28-d air-cured strength of each mixture was used as the reference strength. Specimens were then kept under water at ~24 °C for another 28 d, removed from water, their surfaces dried using a towel, and tested without delay (within minutes).

3. RESULTS AND DISCUSSION

3.1 Setting times of oxalate mortars

The setting times of the mixtures are given in Table 3.

TABLE 3. Final setting times of mixtures with and without the retarder.

Mixtures	Setting time without borax (min.)	Setting time with borax (min.)
MgOx-6/4	5.5	11.0
MgOx-7/3	6.5	12.0
SlOx-6/4	1.0	5.0
SlOx-7/3	1.0	6.0
MgSlOx	2.0	5.0

SlOx mixtures have shorter setting times than MgOx mixtures. The alkaline powder reacted with the acid salt affects the initial pH of oxalate cement pastes (Figure 5), which changes the relative amounts of the different oxalate species present in the solution. SlOx pastes have higher initial pH and form calcium oxalates while MgOx have lower initial pH and form magnesium oxalates, resulting in the observed differences in setting time. Addition of borax prolongs setting times of all mixtures. The mechanism is likely similar for MgOx and SlOx to the retardation it causes in MPCs. At low pH, tetraborate ions from borax dissolution are adsorbed on the surface of MgO particles. This produces a layer which slows the dissolution of MgO (52).

3.2. Influence of mixture proportions on strength development

The strength development of the mortars are compared in Figure 4.

The very early-age (4 h) strengths of both types of mortars are < 8 MPa. Although this appears low in comparison with the analogous MPC, most such high early strengths reported for MPC are measured on pastes, which allows very low W/B to be employed (20, 24). Initial comparisons indicate that oxalate cements have slightly greater water need than phosphate cements. 1-d strength is higher for MgOx than SlOx, reaching ~17.5 MPa for MgOx-7/3. The higher amount of borax used in the SlOx mixtures contributes to the lower early strength. Borax not only retards the reactions but also contributes some water (W/B becomes ~0.31 and ~0.33 for mixtures with 5 % and 10 % borax). MgOx mortars reach their ultimate strengths at ~7 d, and MgOx-7/3 even shows a slight drop in strength beyond 7 d. The fact that MgOx-6/4, which reaches > 30 MPa ultimate strength, does not show a similar drop in strength

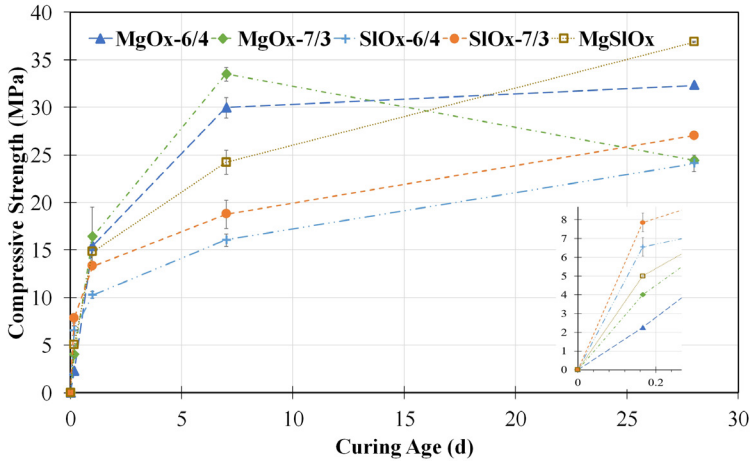

FIGURE 4. Compressive strength development of MgOx and SlOx mortars (inset shows the first 4 h).

after 7 d, suggests a critical magnesium-to-oxalate ratio may have been exceeded in MgOx-7/3, leading to volume instabilities. The strength of SlOx mortars reach 24-27 MPa, and MgSlOx, with an equal mass combination of the two alkaline powders has the highest 28-d strength among all mortars. More importantly, the strengths of all slag-containing mortars have an upward trend from 7 d to 28 d, indicating their ultimate strengths may be even higher. Much as early-age strength gain is related with the formation of crystalline reaction products, later-age strength is related with the formation of pore-filling amorphous phases and this may explain the delayed but continuing strength gain of slag-bearing mortars.

3.3. Change in pH

The change in the pH of the pastes is compared in Figure 5. The increase of the low initial pH of acid-base paste mixtures is related with the amount of reaction hence corresponding neutralization.

The initial pH of FAOx in water is low (~1), due to the dissolution of oxalates in water. MgOx pastes have lower initial pH (1-2) than SlOx pastes (~4). Initial pH is related to early mortar strength, higher for SlOx than MgOx. For both mixture types, pH quickly rises as Mg^{2+} and Ca^{2+} from the dissolution of the alkaline powders react with the available oxalate species (the oxalate and hydrogen oxalate anions). The pH of MgOx rises quickly to 8-9 within 24 h, after which it more or less plateaus, similar to the pH development reported for ferrous oxalate cement pastes (39). The rise in pH is much less for SlOx, only to ~5, suggesting less complete neutralization reactions, and explaining the lower 7 or 28 d strengths. Despite little change in pH after 1 h for SlOx pastes, strength increases up to 28 d (Figure 4). The moderately acidic environment is hence suitable for continued dissolution of slag particles and formation of more reaction products. The ultimate pH of MgSlOx paste is ~7, in between the values for MgO1500-only and slag-only pastes. This neutral value suggests a better balance between acidic and alkaline starting powders and a lower amount of materials left unreacted after the rapid reactions.

3.4. Influence of mixture proportions on mineralogy

Figure 6 compares the mineralogical development of the pastes. MgOx pastes, as expected, contain a hydrated magnesium oxalate, glushinskite ($MgC_2O_4 \cdot 2H_2O$) as their main reaction products. Whewellite ($CaC_2O_4 \cdot H_2O$) and quartz are also found in the final paste. Quartz carries from the unreacted part of FAOx. Whewellite is also present in FAOx but it is not clear whether it partly dissolves in the acidic condition achieved when FAOx is added to water and then reforms as pH increases. Also present are unreacted magnesia (periclase) and forsterite, coming from MgO1500. Small amounts of magnesiowüstite ($Fe_xMg_{1-x}O$), and magnesioferrite (Fe_2MgO_4) are also detected but their peaks partly overlap with those of whewellite and forsterite. The diffractograms of the SlOx pastes suggest whewellite and another calcium oxalate, weddellite ($CaC_2O_4 \cdot 2H_2O$), as well as a small amount of portlandite.

MAUD (53) was used to analyze the 28-d XRD spectra using the Rietveld method. Glushinskite, whewellite, periclase, quartz, and forsterite were considered as the only phases existing in MgOx pastes. Whewellite, weddellite, quartz, and portlandite are considered as the crystalline phases in SlOx, with additional amorphous content. Diffraction data of the selected phases taken from the "crystallography open database" were loaded into MAUD. Background substraction, scaling, and noise cancellation

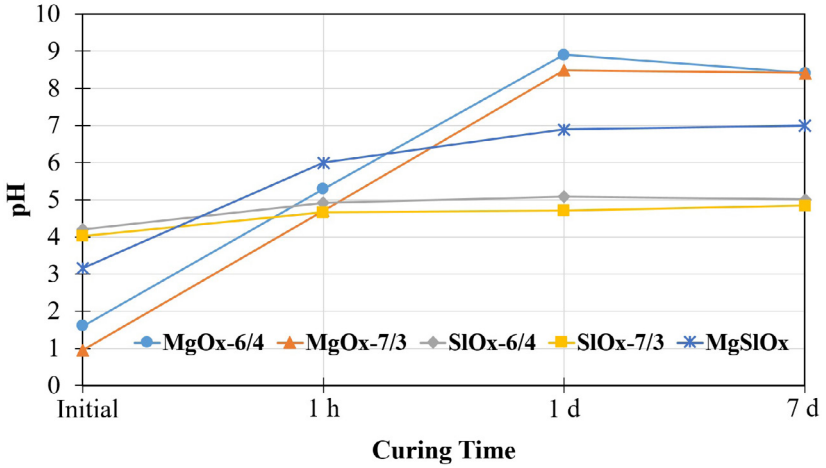

Figure 5. Change in pH for the paste samples.

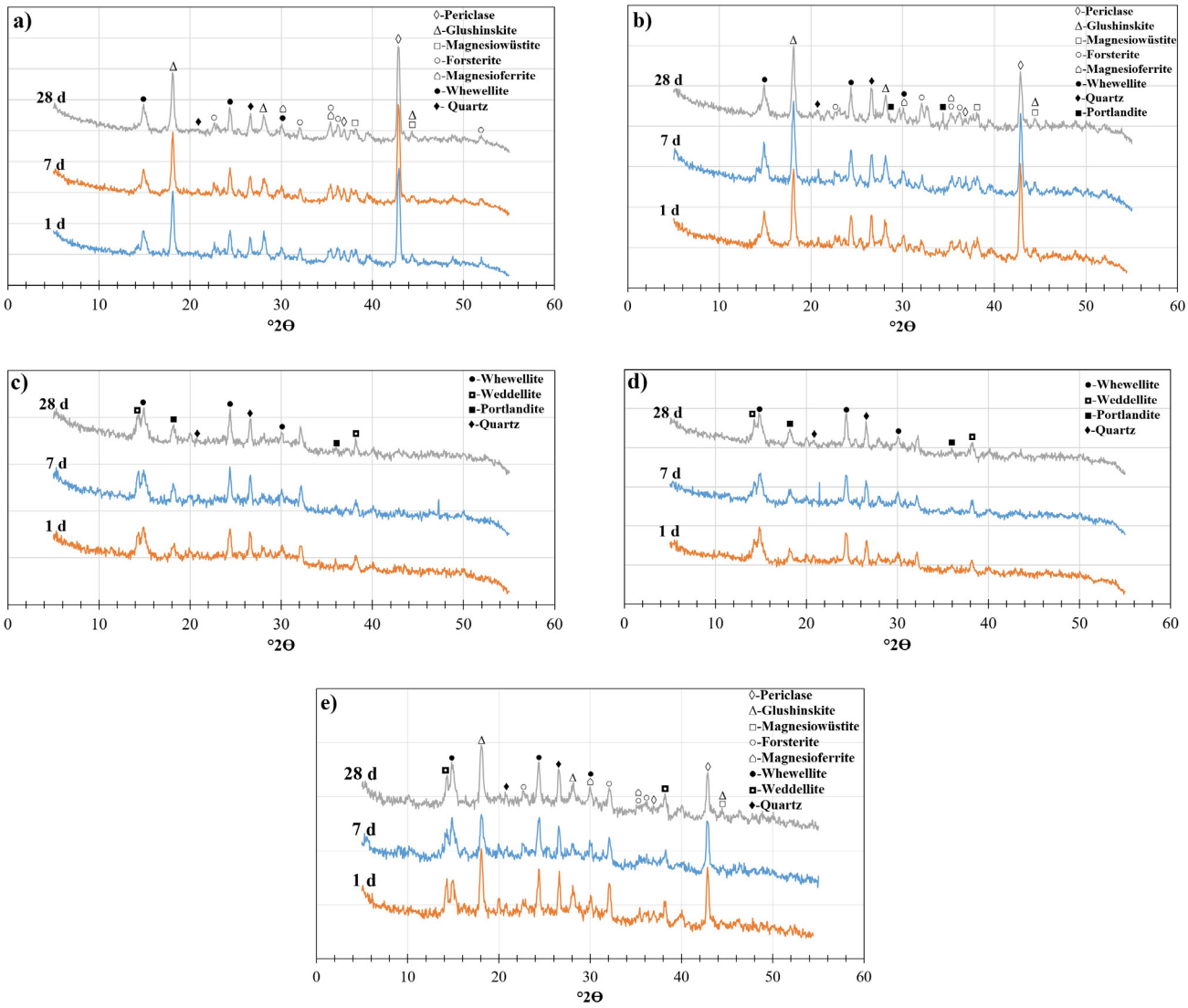

Figure 6. XRD of MgOx and SlOx pastes. a) MgOx-6/4; b) MgOx-7/3; c) SlOx-6/4; d) SlOx-7/3; e) MgSlOx.

operations were performed. Analysis of MgOx-6/4 suggested ~35 % glushinskite, ~20 % whewellite, and ~25 % periclase, as well as ~4 % quartz and ~16 % forsterite. The fit parameter, R_w, was 7.1 %. The amorphous content of MgOx pastes was determined, using an internal standard, to be negligible. For MgOx-7/3, slightly greater amounts of the oxalates (~40 % glushinskite and ~25 % whewellite), and less periclase (~18 %) are calculated, consistent with its higher FAOx/MgO1500. The amounts of the remnant phases also change as expected, quartz increases to 5 % and forsterite decreases to 11 %. R_w was calculated as 8.9 %. Further inspection of these results suggested that the calculated amounts of phases may be slightly under/overestimated. The amount of non-volatile oxides in the starting mixture should equal their amounts in the final paste. For example, in the starting mixture for MgOx-6/4, MgO is mostly in MgO1500, SiO_2 is in MgO1500 (in Forsterite) and in FAOx (from FA), while CaO and C_2O_4 are mostly in FAOx. Since the amounts of each material in the starting mixture is known (Table 2), using the oxide composition for each (Table 1), and assuming FAOx contains 49 % FA and 51 % C_2O_4 (verified approximately by XRF tests), the amounts of glushinskite, whewellite, periclase, quartz, and forsterite (total 100 %) that best satisfy the "mass of oxide in initial mixture equals mass of oxide in final paste" objective for MgO, SiO_2, CaO, and C_2O_4 are calculated using the Solver add-in program in MS Excel as 35 %, 22 %, 18 %, 11 %, 14 %. Hence, there is probably a smaller amount of (unreacted) periclase and a greater amount of quartz in the reacted paste than quantified from the diffractogram in Figure 6a. The same analysis for MgOx-7/3 calculates 38 %, 25 %, 10 %, 11 %, 14 % for of glushin-

skite, whewellite, periclase, quartz, and forsterite, again suggesting unreacted periclase was initially overestimated and quartz was underestimated. This may be partly related with certain minor phases not being considered for the quantification or measurement parameters leading to insufficient intensity for some peaks i.e. low signal-to-noise ratio. Reviewing these calculated amounts of each phase and Tables 1 and 2, it can be deduced that the amount of forsterite increases while quartz decreases from the starting mixture to the final paste. Hence, some of the quartz in FAOx (from FA) reacts with dissolved MgO1500 to form new forsterite. It is unclear whether the forsterite initially available in MgO1500 ever partly dissolves in the acidic solution. This makes it difficult to calculate a degree of reaction for MgO1500. However, the initial fractions of MgO1500 in the starting mixture and the final unreacted periclase contents indicate that the degree of reaction of MgO1500 is higher in MgOx-7/3 than in MgOx-6/4, consistent with its higher 7-d strength (Figure 4, ignoring the subsequent drop in strength due to durability problems). Tracking MgO only (starting in MgO1500 and ending up in Glushinskite, Forsterite, and unreacted Mg1500), degrees of hydration for MgO1500 in MgOx-6/4 and MgOx-7/3 are 45 % and 55 %, respectively. Similar low degrees of reaction for MgO have been reported for magnesium phosphate cements (54). The amorphous natures of the slag and some reaction products complicate the quantitative interpretation of XRD for the SlOx and MgSlOx pastes. The amorphous content in SlOx-7/3 is determined as ~45 %. Even if the slag used is fully amorphous, this would mean part of the reaction products, ~20 % of the total mass, is amorphous as well. The weddellite/whewellite ratio is higher in SlOx-6/4 than in SlOx-7/3 as expected due to its lower FAOx content (Figures 6c and d). Whewellite is the more stable one of the two calcium oxalates. The initial crystallization phase from aqueous solution is a calcium oxalate trihydrate, which loses water of crystallization to either the monohydrate or dihydrate, depending on conditions, such as the calcium to oxalate ion ratio or the presence of substances which form complexes with either calcium or oxalate ions, such as citric acid and magnesium (55). Weddellite precipitates under excess of calcium ions in the medium. This is consistent with no weddellite being detected in MgSlOx, which contained much less slag, hence much less calcium, than either SlOx. The total whewellite and weddellite content is ~46 % in SlOx-6/4 and ~49 % in SlOx-7/3. The total amount of whewellite and weddellite that can be formed can be estimated considering the total calcium in the slag and in the fly ash used to produce FAOx. 1 g of the slag in Table 1 can produce 1.06 g whewellite or 1.17 g weddellite. Similarly, 1 g of FA in Table 1 can produce 0.60 g whewellite or 0.66 g weddellite. Assuming equal amounts of each are formed, the maximum total amount of whewellite and weddellite that can be produced in SlOx-6/4 is calculated as ~49 %. Although the calculated total is below this value, it is probably high, since it is unlikely that all the calcium forms one of the two calcium oxalates.

3.5. Thermogravimetric analyses

Figure 7 presents the mass loss and heat flow measured for paste samples heated to 900 °C.

Mass loss takes place in three main steps for all pastes, which contrasts with the one step decomposition of K-struvite in MPCs (56). Although glushinskite decomposes in two steps, the presence of whewellite coming from FAOx in the MgOx pastes causes a third mass loss step. Figure 8 summarizes the decomposition steps for the calcium and magnesium oxalates and the theoretical mass losses associated with each step (57-59).

Up to ~100 °C, mass loss is related with free water in all pastes. The rest of the mass loss in step 1 is due to loss of crystal water in the magnesium and calcium oxalates. Figures 7b and 7f show two mass loss peaks for MgOx, one at 150 °C due to the decomposition of whewellite and another at 210-220 °C (higher than suggested in Figure 8). For SlOx, the dominant loss peak is at ~160 °C, as expected for whewellite (Figures 7d and 7h). Although XRD suggests presence of weddellite, a related lower temperature peak is not observed. The second step (400-500 °C) is related with the decomposition of anhydrous magnesium and calcium oxalates. The break-down of MgC_2O_4 releases CO and CO_2 leaving behind MgO. Decomposition of CaC_2O_4 releases CO and leaves behind $CaCO_3$. The main peaks for SlOx (whewellite decomposition) in this step have shoulder peaks (weddellite decomposition) on their lower temperature sides, most noticeable for SlOx-7/3, in Figure 7h. The third step (600-800 °C) breaks down the remaining carbonate, releasing CO_2.

3.6. Influence of mixture proportioning on the microstructure

Figure 9 presents SEM images of reacted pastes.

Many loosely connected prismatic crystals of 4-5 μm size are observed in MgOx-6/4 among unreacted magnesia particles (Figure 9a). Crystals in MgOx-7/3 are smaller and cube-like (Figure 9b). SlOx shows smaller, mostly sub-micrometer crystals dispersed in a glassy background (Figures 9c and 9d). Notably, cracks are observed in MgOx-7/3 (Figure 9b), which could explain the strength loss recorded for this mixture from 7 to 28 d. In MgSlOx (Figure 9e), the amorphous material produced by reactions of the slag envelops the crystals, leading to a

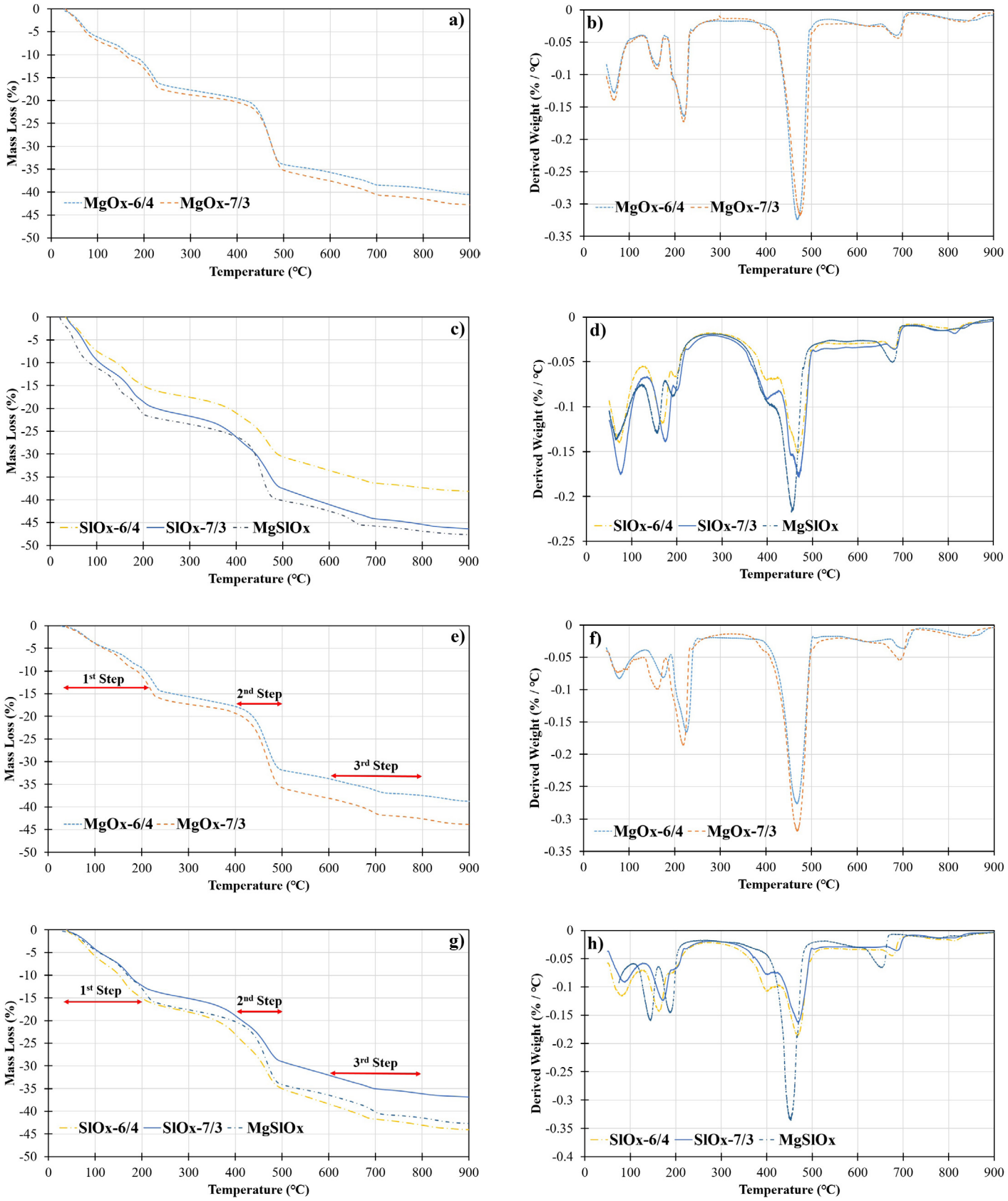

Figure 7. Mass loss and corresponding derived weight curves at. (a,b,c,d) 1 d; (e,f,g,h) 35 d.

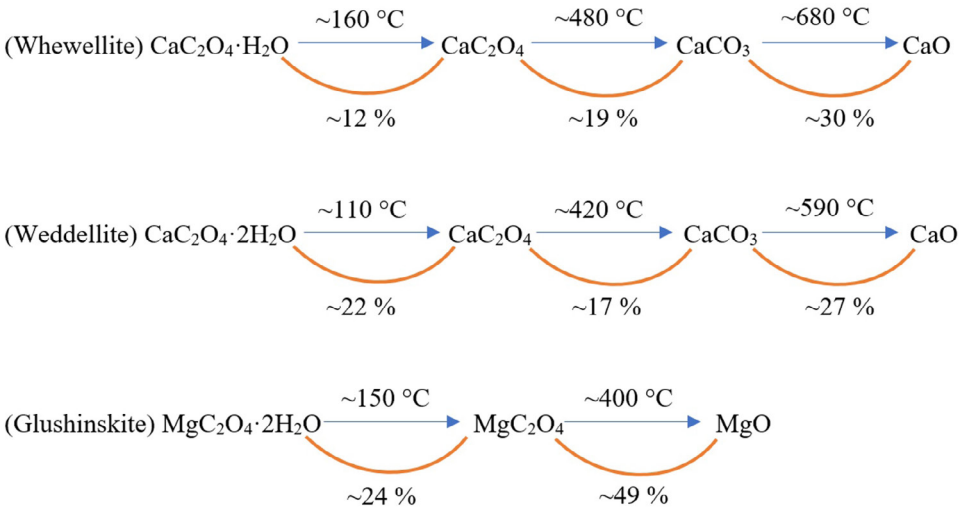

Figure 8. Thermal decomposition of oxalate minerals (losses are percentage of initial mineral mass).

denser microstructure explaining the higher ultimate strength measured on mortar samples.

3.7. Pore size distribution and porosity

Figure 10 presents the pore size distributions of the prepared pastes.

MgOx-6/4 has the lowest porosity (Figure 10a) among all mixtures. MgOx-7/3 has the highest of all mixtures which could be related with the cracks observed in Figure 9b. This paste also contains an unexpectedly high amount of pores of nearly 1 µm size which could be microcracks. All samples appear to contain two dominant sizes of pores, larger than ~0.1 µm and smaller than ~0.02 µm. Both MgOx pastes have greater average pore size than SlOx samples, as well as a wider range of pore sizes. The amorphous products in the slag-containing pastes may be refining their larger pores. Differences in the amount of small and large pores in Figure 10 may explain the differences in strength better than total porosity. MgSlOx, the paste with the highest

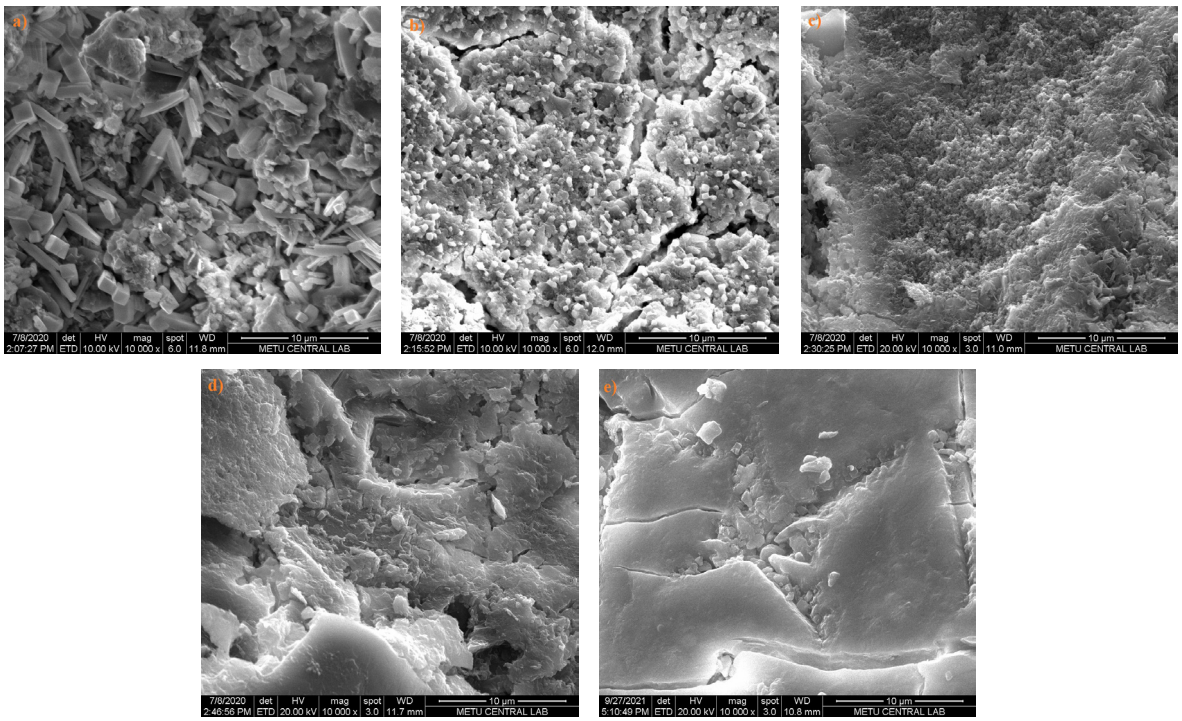

Figure 9. SEM images of the pastes. a) MgOx-6/4; b) MgOx-7/3; c) SlOx-6/4; d) SlOx-7/3; e) MgSlOx.

strength, has a smaller amount of such large pores and a greater amount of smaller pores.

3.8. Temperature changes

There are two distinct heat-evolving steps in the reactions of MgOx and SlOx: i) the wetting and dissolution of FAOx in water, and ii) the contact of the alkaline powder (MgO1500 or slag) with the FAOx and water mixture. The contact of the alkaline powder alone with water evolves heat but is insignificant in comparison with the other two steps. Figure 11a shows the change in temperature of the various oxalate pastes prepared. Temperature rises sharply by 7-8 °C when FAOx and water are mixed (time zero). This is considerable for the small paste volume (~7 cm^3) used. After ~1 min, the slurry begins to cool slowly.

The addition of the alkaline powder creates a second (maximum) temperature peak. The time delay of the alkaline powder addition affects this maximum temperature. Figure 11b shows the change in this maximum temperature with the amount of time elapsed before adding the alkaline powder. A longer wait period reduces the overlap of the two separate heat-evolving events, and a slightly lower maximum temperature is recorded. However, the FAOx + water paste begins to stiffen in time hence a very long wait period may require additional water to be added, influencing hardened properties. MgOx pastes reach slightly higher temperatures than SlOx. The temperature peak occurs 2-3 min after all materials have been added. Hence, setting which takes place after 5-10 minutes follows the temperature peak with a minor delay.

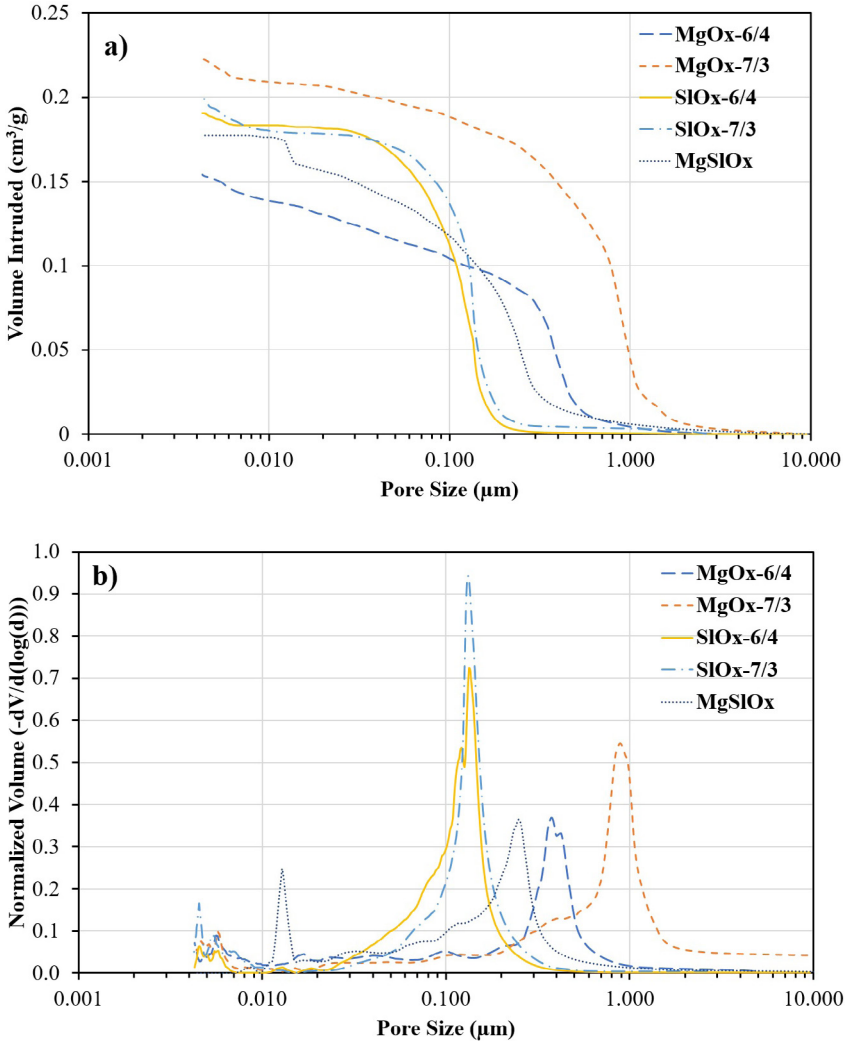

Figure 10. Pore size distribution curves obtained by mercury intrusion porosimetry. a) Total volume intruded vs. Pore size; b) Normalized volume vs. Pore size.

3.9. Water resistance

The resistance of MgOx, SlOx, and MgSlOx mortars to water are compared in Figure 12. MgOx mortars cured in air and then kept under water do not show significant changes in compressive strength (observed differences being within experimental uncertainty). In contrast, both SlOx mortars lose ~70 % of their air-dried strengths. This decrease could be related with the dissolution of the reaction products present. Hydraulic pressure inside pores within the sample could also negatively affect strength since these samples are tested immediately after removal from water, without any time to dry. Small increases in the strengths of MgOx-6/4 and MgSlOx may be due to continued reaction in mortars which had not reached their ultimate strengths prior to submersion in water.

3.10. Reaction mechanism of magnesium/calcium oxalate cements

There are two main steps in the reaction of MgOx cements with water. In the first step, the dissolution of FAOx in water yields oxalate ion species and H^+, which makes the solution acidic. A diprotic acid, oxalic acid has $pKa_1 = 1.27$ and $pKa_2 = 4.27$. Hence, at the initial low pH of ~2 (Figure 5) more $HC_2O_4^-$ and some $H_2C_2O_4$ are present in the solution (39).

$$H_2C_2O_4 \rightarrow H^+ + HC_2O_4^- \ (pK_{a1} = 1.27) \qquad [1]$$

In the second step, the periclase in MgO1500 begins to dissociate in the acidic solution and reacts with $HC_2O_4^-$. pH rises and $HC_2O_4^-$ further dissociates into $C_2O_4^{2-}$. At pH~4-4.5, approximately equal amounts of $HC_2O_4^-$ and $C_2O_4^{2-}$ are present in the solution (39).

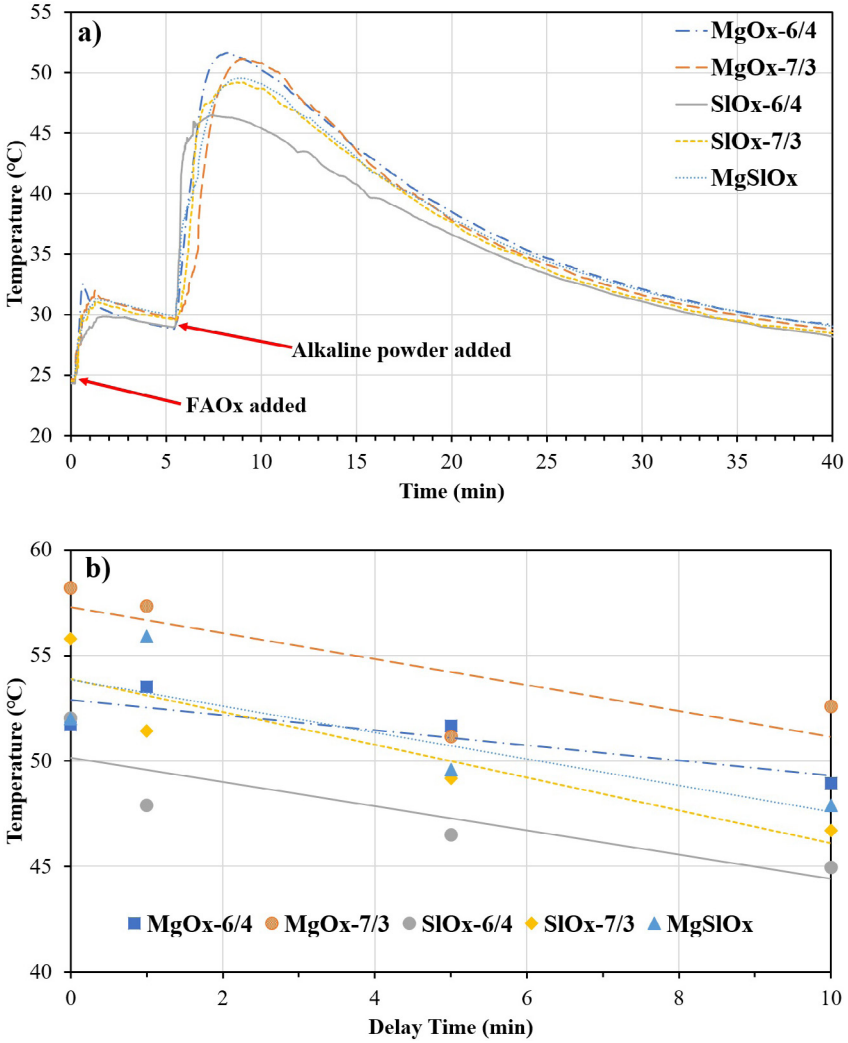

Figure 11. a) Change in the temperature of the paste samples (5 min delay between addition of FAOx and alkaline powder); b) Maximum temperature of paste samples vs. time delay between adding FAOx and adding alkaline powder (lines are the best-fits to the data points for each paste).

$$HC_2O_4^- \rightarrow H^+ + C_2O_4^{2-} \ (pK_{a2} = 4.27) \quad [2]$$

The continued dissolution of MgO1500 (forsterite and periclase) releases amorphous silica and Mg^{2+} into solution (60), resulting in a rapid increase in pH (the first hour in Figure 5). $HC_2O_4^-$ and $C_2O_4^{2-}$ react with the Mg^{2+} ions to form glushinskite (Figures 6a and 6b):

$$MgO + 2H^+ \rightarrow Mg^{2+} + H_2O \quad [3]$$
$$Mg^{2+} + HC_2O_4^- + 2H_2O \rightarrow MgC_2O_4.2H_2O + H^+ \quad [4]$$
$$Mg^{2+} + C_2O_4^{2-} + 2H_2O \rightarrow MgC_2O_4.2H_2O \quad [5]$$

The role of Eqns. 4 and 5 in glushinskite formation depends on pH. As pH increases, Equation 5 predominates and glushinskite continues to precipitate at a slowing pace. Unreacted periclase is found in the final solid, as well as quartz and whewellite ($CaC_2O_4.H_2O$) remaining from unreacted FAOx. In the case of SlOx, the reaction of slag in FAOx + water begins at pH ~ 4-5 where $C_2O_4^{2-}$ is abundant in the solution. The acidic conditions lead to dissolution of Ca^{2+} from the slag which react with $C_2O_4^{2-}$ to form weddellite (Figures 6c and 6d). Calcium ions can also come from whewellite in FAOx, the solubility of which increases markedly at pH < 5 (61). The reactions in SlOx can be simplified as:

$$CaO + 2H^+ \rightarrow Ca^{2+} + H_2O \quad [6]$$
$$Ca^{2+} + C_2O_4^{2-} + 2H_2O \rightarrow CaC_2O_4.2H_2O \quad [7]$$

3.11. Carbon neutrality and feasibility of MgOx and SlOx cements

The argument that oxalate cements can be carbon neutral or even negative relies on the availability of oxalic acid produced from captured CO_2. Hence, a natural supposition is that carbon-negative oxalate cements would be cost-prohibitive. Although production of oxalic acid from CO_2 has been shown at the laboratory scale, since no large-scale production exists, the overall cost of this step is not easy to predict (15). However, simple calculations and various assumptions can be used to estimate a rough cost and carbon footprint for MgOx and SlOx systems. The production of the alkaline powder is the main contributor to the carbon emissions related with oxalate cements. As stated in Section 2.2, ~1.5 g chemical and fuel related CO_2 is emitted during the production of 1 g dead-burned MgO from pure $MgCO_3$. Hence, FAOx:MgO1500 must be greater than 3 to obtain a carbon neutral or negative mixture. The CO_2 emissions related with grinding, which are relatively small (62) or with the preparation of FAOx (mainly heating and grinding) can further increase this ratio. Conversely, this ratio can decrease if the MgO used has a low carbon footprint, like one derived from seawater (63) is used, or if a higher OxAc:FA is used to prepare FAOx. However, varying OxAc:FA causes changes in the rate and heat of reaction of the overall system. When slag is used as the alkaline powder, the main factor that increases the CO_2 footprint becomes the grinding of granulated slag. Since the oxalate salt portion of the system remains unchanged, SlOx cements can be carbon negative, as long as the emissions due to grinding are below 1 g CO_2 per 1 g ground slag. This reinforces the importance of identifying a low-carbon-footprint alkaline powder to replace dead-burned MgO in making oxalate cements.

The cost of MgSlOx concrete is assessed (Table 4) by making assumptions about the unit costs of various materials or operations (15). 300 kg of powder (MgO1500+slag+FAOx) is assumed per 1 m^3 of concrete. Using the proportions in Table 2, 210 kg of the powder is FAOx, so ~153.3 kg OxAc (dihydrate) is needed (~0.73 g OxAc is required to make 1 g of the FAOx in this study). The production of OxAc from

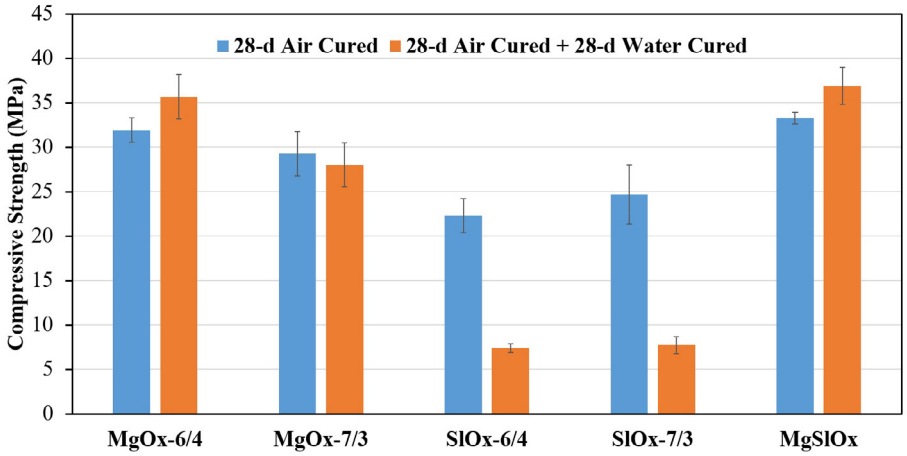

Figure 12. The strengths 28-d air-cured samples and their retained strengths after additional 28-d water-curing.

TABLE 4. Simple cost analysis for 1 m^3 MgSlOx concrete.

Material /process	Amount in concrete (kg/m^3)	Unit price ($/t)			Estimated cost ($/$m^3$)		
		Low	Intermediate	High	Low	Intermediate	High
OxAc (includes CO_2 capture)	107.1 (from 153.3 kg $H_2C_2O_4.2H_2O$)	450	750	1100	69.0	115.0	168.6
MgO1500	45		150			6.8	
Slag	45		20			0.9	
Borax	15		500			7.5	
FA	102.9		20			2.1	
Production of FAOx (heating 210 kg/m^3)	-		15			3.2	
Aggregates	2000		10			20	
Water	150		5			0.8	
Total	2465		-		110.1	156.1	209.8

CO_2 is not done at a large scale outside of the lab, so it is most difficult to assign a cost to this process. The current cost of sustainable OxAc production from CO_2 (including the cost of CO_2) was estimated in a European research Project (34) as > 1100 $/t. However the cost was projected to drop to < 450 $/t beyond 2030, with lower or negative CO_2 cost (with incentives), a reduction in cell cost, and improved current densities, and a reduced electricity price. Another study (31) estimated the cost of electrochemical production of OxAc from CO_2 as being equal to the market price of oxalic acid made from other sources, which can be taken as 450-600 $/t (64). They did not include the cost of capturing CO_2 needed to produce OxAc which is also difficult to estimate. As an example, for one of the methods, direct air capture, Keith et al. (65) estimate levelized costs of 94-232 $/t. Based on these studies, 450 $/t, 750 $/t, and 1100 $/t are chosen as the unit price of OxAc made from captured CO_2. Hence, the cost of OxAc used to produce MgSlOx concrete becomes 69-168.6 $/$m^3$.

A low-purity MgO1500 obtained like the one in this study, assumed to cost 150 $/t (66), adds another 6.8 $/$m^3$ (four tenths of the powder binder is MgO1500). Costs of 20 $/t for ground slag (67), 10 $/t for aggregates, 5 $/t for mixing water (W/B = 0.5), and 500 $/t for borax are assumed. The cost of 102.9 kg/m^3 FA (~49 % of FAOx) is assumed to be 2.1 $/$m^3$ even though the FA in this study is a waste (not suitable for PC concrete). The production cost of FAOx is assumed as 15 $/t by comparison with similar low-temperature processes (e.g. production of gypsum) which adds another 3.2 $/$m^3$ (for 210 kg/m^3 FAOx). The total cost of MgSlOx concrete becomes ~110-210 $/$m^3$. This does not consider mixing, delivery etc. which would have to differ from PC systems because of differences in properties like setting time, or profit. Similar calculations for MgOx-6/4 yield a cost range of 110-195 $/$m^3$, slightly lower because of the decreased amount of oxalic acid used. In comparison, ready-mixed concrete can cost > 150 $ in many developed countries (68). These calculations show that the cost of oxalate cement is dominated by the cost of producing oxalates from captured CO_2 and that changing the alkaline powder does not influence cost as much as it does the carbon footprint. Nevertheless, the identification of an effective low-carbon base may allow the amount of OxAc in these systems to be slightly reduced and still achieve carbon neutrality (e.g. FAOx/basic powder < 6:4) which could further decrease the overall cost.

4. CONCLUSIONS

The development of oxalate cements made with ground granulated blast furnace slag were introduced and compared with magnesium oxalate cements. The following conclusions were reached:

- The setting times of SlOx are shorter than those of MgOx. The use of borax can increase setting time > 10 min for MgOx.
- The final products in both systems are hydrated oxalates and unreacted raw materials. MgOx

contains glushinskite and whewellite, while SlOx contains whewellite and weddellite. Microscopy reveals prismatic crystals of 3-5 µm size in MgOx. Slag-containing pastes contain smaller crystals in a glassy background.
- Unlike MgOx mortars which show greater early strength, SlOx mortars continue to gain strength beyond 7 d. MgSlOx hybrid mortar reaches ~37 MPa, the highest strength at 28 d.
- SlOx contains smaller pores (< 0.2 µm) than MgOx (< 1 µm). Despite their smaller pores, the resistance of SlOx to water is significantly lower than MgOx or MgSlOx.
- The final pH of the pastes is ~9 for MgOx and ~5 for SlOx. An equal part combination of the two alkaline powders gives MgSlOx a pH of ~7, indicating a better balance between acidic and alkaline components.
- Both slag and dead-burned magnesia can be reacted with oxalic acid salts to yield a fast-setting cement paste or mortar with medium strength. Replacement of dead-burned magnesia with slag reduces the CO_2 footprint of the binder, which can be truly carbon neutral if made using oxalic acid made from captured CO_2.

ACKNOWLEDGEMENTS

This research did not receive any specific grant from funding agencies in the public, commercial, or not-for-profit sectors.

AUTHOR CONTRIBUTIONS:

Conceptualization: S.T. Erdoğan. Investigation: S.T. Erdoğan, B.A. Bilginer. Methodology: S.T. Erdoğan, B.A. Bilginer. Supervision: S.T. Erdoğan. Writing, original draft: S.T. Erdoğan, B. A. Bilginer. Writing, review & editing: S.T. Erdoğan, B.A. Bilginer.

REFERENCES

1. Mehta, P.K.; Monteiro, P.J.M. (2014) Concrete: microstructure, properties, and materials. fourth ed., McGraw-Hill Education, New York, USA.
2. Glasser, F.P.; Zhang, L. (2001) High-performance cement matrices based on calcium sulfoaluminate - belite compositions. *Cem. Concr. Res.* 31 [12], 1881-1886. https://doi.org/10.1016/S0008-8846(01)00649-4.
3. Canbek, O.; Shakouri, S.; Erdoğan, S.T. (2020) Laboratory production of calcium sulfoaluminate cements with high industrial waste content. *Cem. Concr. Compos*. 106, 103475. https://doi.org/10.1016/j.cemconcomp.2019.103475.
4. Scrivener, K.; Martirena, F.; Bishnoi, S.; Maity, S. (2018) Calcined clay limestone cements (LC^3). *Cem. Concr. Res*. 114, 49-56. https://doi.org/10.1016/j.cemconres.2017.08.017.
5. Aziz, A.; Driouich, A.; Bellil, A.; Ali, M.B.; Mabtouti, S.E.L.; Felaous, K.; Achab, M.; El Bouari, A. (2021) Optimization of new eco-material synthesis obtained by phosphoric acid attack of natural Moroccan pozzolan using Box-Behnken Design. *Ceram. Int.* 47 [23], 33028-33038. https://doi.org/10.1016/j.ceramint.2021.08.203.
6. Pachideh, G.; Gholhaki, M.; Ketabdari, H. (2020) Effect of pozzolanic wastes on mechanical properties, durability and microstructure of the cementitious mortars. *J. Build. Eng.* 29, 101178. https://doi.org/10.1016/j.jobe.2020.101178.
7. Sumesh, M.; Alengaram, U.J.; Jumaat, M.Z.; Mo, K.H.; Singh, R.; Nayaka, R.R.; Srinivas, K. (2021) Chemo-physico-mechanical characteristics of high-strength alkali-activated mortar containing non-traditional supplementary cementitious materials. *J. Build. Eng.* 44, 103368. https://doi.org/10.1016/j.jobe.2021.103368.
8. Davidovits, J. (2008) Geopolymer chemistry and applications, third ed., Institut Géopolymère, St. Quentin, France.
9. Borštnar, M.; Daneu, N.; Dolenec, S. (2020) Phase development and hydration kinetics of belite-calcium sulfoaluminate cements at different curing temperatures. *Ceram. Int.* 46 [18], 29421-29428. https://doi.org/10.1016/j.ceramint.2020.05.029.
10. Habert, G.; d'Espinose de Lacaillerie, J.B.; Roussel, N. (2011) An environmental evaluation of geopolymer based concrete production: reviewing current research trends. *J. Clean. Prod.* 19 [11], 1229-1238. https://doi.org/10.1016/j.jclepro.2011.03.012.
11. Meyer, V.; de Cristofaro, N.; Bryant, J.; Sahu, S. (2018) Solidia cement an example of carbon capture and utilization. *Key Eng. Mater.* 761, 197-203. https://doi.org/10.4028/www.scientific.net/kem.761.197.
12. Carbon Built. Retrieved from: https://www.carbonbuilt.com (accessed 03 January 2023).
13. Criado, Y.A.; Arias, B.; Abanades, J.C. (2018) Effect of the carbonation temperature on the CO_2 carrying capacity of CaO. *Ind. Eng. Chem. Res*. 57, 12595-12599. https://doi.org/10.1021/acs.iecr.8b02111.
14. Niven, R.; Monkman, G.S.; Forgeron, D. (2012) US Patent 8,845,940 B2, Carbon dioxide treatment of concrete upstream from product mold. Retrieved from: https://patents.google.com/patent/US8845940B2/en.
15. Erdoğan, S.T.; Bilginer, B.A.; Canbek, O. (2022) Preparation and characterization of magnesium oxalate cement. *Engrxiv.* https://doi.org/10.31224/2298.
16. Erdoğan, S.T. (2017) Oxalate acid-base cements as a means of carbon storage. American Geophysical Union Fall Meeting 2017, New Orleans, 11-15 December 2017.
17. Erdoğan, S.T. (2019) Magnesium oxalate cements for carbon reuse. American Geophysical Union Fall Meeting 2019, San Francisco, 9-13 December 2019.
18. İçinsel, N. (2020) Development of magnesium oxalate cements with recycled portland cement paste. M.S. Thesis, Middle East Technical University, Ankara, Turkey.
19. Liu, Y.; Chen, B. (2019) Research on the preparation and properties of a novel grouting material based on magnesium phosphate cement. *Constr. Build. Mater.* 214, 516-526. https://doi.org/10.1016/j.conbuildmat.2019.04.158.
20. Haque, M.A.; Chen, B.; Maierdan, Y. (2022) Influence of supplementary materials on the early age hydration reactions and microstructural progress of magnesium phosphate cement matrices. *J. Clean. Prod.* 333, 130086. https://doi.org/10.1016/j.jclepro.2021.130086.
21. Haque, M.A.; Chen, B.; Javed, M.F.; Jalal, F.E. (2022) Evaluating the mechanical strength prediction performances of fly ash-based MPC mortar with artificial intelligence approaches. *J. Clean. Prod.* 355, 131815. https://doi.org/10.1016/j.jclepro.2022.131815.
22. Haque, M.A.; Chen, B.; Liu, Y.; Farasat Ali Shah, S.; Ahmad, M.R. (2020) Improvement of physico-mechanical and microstructural properties of magnesium phosphate cement composites comprising with Phosphogypsum. *J. Clean. Prod.* 261, 121268. https://doi.org/10.1016/j.jclepro.2020.121268.
23. Yang, N.; Shi, C.; Yang, J.; Chang, Y. (2014) Research progresses in magnesium phosphate cement based materials. *J. Mater. Civil Eng*. 26 [10]. https://doi.org/10.1061/(ASCE)MT.1943-5533.0000971.
24. Mestres, G.; Ginebra, M.P. (2011) Novel magnesium phosphate cements with high early strength and antibacterial properties. *Acta Biomater.* 7 [4], 1853-1861. https://doi.org/10.1016/j.actbio.2010.12.008.
25. Buj, I.; Torras, J.; Casellas, D.; Rovira, M.; de Pablo, J. (2009) Effect of heavy metals and water content on the strength of magnesium phosphate cements. *J. Hazard. Mater.* 170 [1], 345-350. https://doi.org/10.1016/j.jhazmat.2009.04.091.
26. Yang, Q.; Zhu, B.; Wu, X. (2000) Characteristics and durability test of magnesium phosphate cement-based

material for rapid repair of concrete. *Mater. Struct.* 33, 229-234. https://doi.org/10.1007/BF02479332.
27. König, M.; Lin, S-H.; Vaes, J.; Pant, D.; Klemm, E. (2021) Integration of aprotic CO_2 reduction to oxalate at a Pb catalyst into a GDE flow cell configuration. *Faraday Discuss.* 230, 360-374. https://doi.org/10.1039/D0FD00141D.
28. Meurs, J.H.H. Method of preparing oxalic acid. WO2016124646A1, 2016. Retrieved from https://patents.google.com/patent/WO2016124646A1/da.
29. Chen, A.; Lin, B.L. (2018) A simple framework for quantifying electrochemical CO_2 fixation. *Joule.* 2 [4], 594-606. https://doi.org/10.1016/j.joule.2018.02.003.
30. Subramanian, S.; Athira, K.R.; Kulandainathan, M.A. (2020) New insights into the electrochemical conversion of CO_2 to oxalate at stainless steel 304 L cathode. *J. CO_2 Util.* 36, 105-115. https://doi.org/10.1016/j.jcou.2019.10.011.
31. Fischer, J.; Lehmann, T.; Heitz, E. (1981) The production of oxalic-acid from CO_2 and H_2O. *J. Appl. Electrochem.* 11, 743-750. https://doi.org/10.1007/BF00615179.
32. Ikeda, S.; Takagi, T.; Ito, K. (1987) Selective formation of formic acid, oxalic acid, and carbon monoxide by electrochemical reduction of carbon dioxide. *Bull. Chem. Soc. Jpn.* 60 [7], 2517-2522. https://doi.org/10.1246/bcsj.60.2517.
33. Angamuthu, R.; Byers, P.; Lutz, M.; Spek, A.L.; Bouwman, E. (2010) Electrocatalytic CO_2 conversion to oxalate by a copper complex. *Science.* 327 [5963], 313-315. https://doi.org/10.1126/science.1177981.
34. Schuler, E.; Demetriou, M.; Shiju, N.R.; Gruter, G.J.M. (2021) Towards Sustainable Oxalic Acid from CO_2 and Biomass. *ChemSusChem.* 14 [18], 3636-3664. https://doi.org/10.1002/cssc.202101272.
35. Lide, D.R. (2007) CRC handbook of chemistry and physics, 88th ed., CRC Press, Florida, USA.
36. Kaufman, D.W.; Kelly, J.P.; Curhan, G.C.; Anderson, T.E.; Dretler, S.P.; Preminger, G.M.; Cave, D.R. (2008) Oxalobacter formigenes may reduce the risk of calcium oxalate kidney stones. *J. Am. Soc. Nephrol.* 19 [6], 1197-1203. https://doi.org/10.1681/ASN.2007101058.
37. Ding, Z.; Fang, Y.; Su, J.F.; Hong, S.; Dong, B. (2020) In situ precipitation for the surface treatment and repair of cement-based materials. *J. Adhes. Sci. Technol.* 34 [11], 1233-1240. https://doi.org/10.1080/01694243.2019.1705143.
38. Arvaniti, E.C.; Lioliou, M.G.; Paraskeva, C.A.; Payatakes, A.C.; Østvold, T.; Koutsoukos, P.G. (2010) Calcium oxalate crystallization on concrete heterogeneities. *Chem. Eng. Res. Des.* 88 [11], 1455-1460. https://doi.org/10.1016/j.cherd.2009.09.013.
39. Luo, Z.; Ma, Y.; He, H.; Mu, W.; Zhou, X.; Liao, W.; Ma, H. (2021) Preparation and characterization of ferrous oxalate cement - A novel acid-base cement. *J. Am. Ceram. Soc.* 104 [2], 1120-1131. https://doi.org/10.1111/jace.17511.
40. Liu, Y.; Chen, B. (2019) Research on the preparation and properties of a novel grouting material based on magnesium phosphate cement. *Constr. Build. Mater.* 214, 516-526. https://doi.org/10.1016/j.conbuildmat.2019.04.158.
41. He, Z.H.; Zhu, H.N.; Shi, J.Y.; Li, J.; Yuan, Q.; Ma, C. (2022) Multi-scale characteristics of magnesium potassium phosphate cement modified by metakaolin. *Ceram. Int.* 48 [9], 12467-12475. https://doi.org/10.1016/j.ceramint.2022.01.112.
42. Ding, Z.; Dong, B.; Xing, F.; Han, N.; Li, Z. (2012) Cementing mechanism of potassium phosphate based magnesium phosphate cement. *Ceram. Int.* 38 [8], 6281-6288. https://doi.org/10.1016/j.ceramint.2012.04.083.
43. Ahmad, M.R.; Chen, B.; Yu, J. (2019) A comprehensive study of basalt fiber reinforced magnesium phosphate cement incorporating ultrafine fly ash. *Compos. B. Eng.* 168, 204-217. https://doi.org/10.1016/j.compositesb.2018.12.065.
44. Bilginer, B.A. (2018) Development of magnesium potassium phosphate cement pastes and mortars incorporating fly ash. M.S. Thesis, Middle East Technical University, Ankara, Turkey.
45. ASTM C618. (2019) Standard specification for coal fly ash and raw or calcined natural pozzolan for use in concrete. ASTM International, West Conshohocken, Philadelphia, Pennsylvania, USA.
46. CEN 197-1. (2012) Cement - Part 1: Compositions and conformity criteria for common cements. Brussels, Belgium.
47. Brindley, G.W.; Hayami, R. (1965) Kinetics and mechanism of formation of forsterite (Mg_2SiO_4) by solid state reaction of MgO and SiO_2. *Phil. Mag.* 12 [117], 505-514. https://doi.org/10.1080/14786436508218896.
48. Benhelal, E.; Zahedi, G.; Shamsaei, E.; Bahadori, A. (2013) Global strategies and potentials to curb CO_2 emissions in cement industry. *J. Clean. Prod.* 51, 142-161. https://doi.org/10.1016/j.jclepro.2012.10.049.
49. ASTM C109. (2020) Standard test method for compressive strength of hydraulic cement mortars (using 2-in. or [50 mm] cube specimens). ASTM International, West Conshohocken, Philadelphia, Pennsylvania, USA.
50. Mahyar, M. (2014) Room-temperature phosphate ceramics made with afşin-elbistan fly ash. M.S. Thesis, Middle East Technical University, Ankara, Turkey.
51. Bopegedera, A.M.R.P.; Nishanthi, K.; Perera, R. (2017) "Greening" a familiar general chemistry experiment: coffee cup calorimetry to determine the enthalpy of neutralization of an acid–base reaction and the specific heat capacity of metals. *J. Chem. Educ.* 94 [4], 494-499. https://doi.org/10.1021/acs.jchemed.6b00189.
52. Ma, C.; Wang, F.; Zhou, H.; Jiang, Z.; Ren, W.; Du, Y. (2021) Effect of early-hydration behavior on rheological properties of borax-admixed magnesium phosphate cement. *Constr. Build. Mater.* 283, 122701. https://doi.org/10.1016/j.conbuildmat.2021.122701.
53. Lutterotti, L. (2000) Maud: a rietveld analysis program designed for the internet and experiment integration. *Acta Cryst. A.* 56, s54. https://doi.org/10.1107/S0108767300021954.
54. Yu, J.; Qian, J.; Wang, F.; Qin, J.H.; Dai, X.B.; You, C.; Jia, X.W. (2020) Study of using dolomite ores as raw materials to produce magnesium phosphate cement. *Constr. Build. Mater.* 253, 119147. https://doi.org/10.1016/j.conbuildmat.2020.119147.
55. Gadd, G.M. (1999) Fungal production of citric and oxalic acid: importance in metal speciation, physiology and biogeochemical processes. *Adv. Microb. Physiol.* 42, 47-92. https://doi.org/10.1016/S0065-2911(08)60165-4.
56. Chauhan, C.K.; Vyas, P.M.; Joshi, M.J. (2011) Growth and characterization of struvite-K crystal, *Cryst. Res. Technol.* 46 [2], 187-194. https://doi.org/10.1002/crat.201000587.
57. Frost, R.L.; Weier, M.L. (2003) Thermal treatment of weddellite - a Raman and infrared emission spectroscopic study. *Thermochim. Acta.* 406 [1-2], 221-232. https://doi.org/10.1016/S0040-6031(03)00259-4.
58. Stephens, W.E. (2012) Whewellite and its key role in living systems. *Geol. Today.* 28 [5], 180-185. https://doi.org/10.1111/j.1365-2451.2012.00849.x.
59. Frost, R.L.; Adebajo, M.; Weier, M.L. (2004) A Raman spectroscopic study of thermally treated glushinskite--the natural magnesium oxalate dihydrate. *Spectrochim. Acta A Mol. Biomol. Spectrosc.* 60 [3], 643-651. https://doi.org/10.1016/S1386-1425(03)00274-9.
60. Qiushi, Z.; Xing, C.; Rui, M.; Shichang, S.; Lin, F.; Junhao, L.; Juan, L. (2021) Solid waste-based magnesium phosphate cements: Preparation, performance and solidification/stabilization mechanism. *Constr. Build. Mater.* 297, 123761. https://doi.org/10.1016/j.conbuildmat.2021.123761.
61. Gadd, G.M. (1999) Fungal production of citric and oxalic acid: importance in metal speciation, physiology and biogeochemical processes. *Adv. Microb. Physiol.* 41, 47-92. https://doi.org/10.1016/S0065-2911(08)60165-4.
62. Chen, C.; Habert, G.; Bouzidi, Y.; Jullien, A. (2010) Environmental impact of cement production: detail of the different processes and cement plant variability evaluation. *J. Clean. Prod.* 18 [5], 478-485. https://doi.org/10.1016/j.jclepro.2009.12.014.
63. Turek, M.; Gnot, W. (1995) Precipitation of magnesium hydroxide from brine. *Ind. Eng. Chem. Res.* 34, 244-250. https://doi.org/10.1021/ie00040a025.
64. Retrieved from: https://www.alibaba.com/product-detail/Oxalic-Acid-Dihydrate-99-6-Price_11000003073704.html?s=p (accessed 3 January 2023).
65. Keith, D.W.; Holmes, G.; St. Angelo, D.; Heidel, K. (2018) A process for capturing CO_2 from the atmosphere. *Joule.* 2 [8], 1573-1594. https://doi.org/10.1016/j.joule.2018.05.006.
66. Retrieved from: https://www.alibaba.com/product-detail/Magnesium-Oxide-Magnesium-Oxide-Magnesium-

Oxide_62443248013.html?spm=a2700.7735675.normal_offer.d_title.37124a0chvbcqw&s=p (accessed 3 January 2023).
67. Retrieved from: https://www.alibaba.com/product-detail/Hot-Sell-China-Granulated-Blast-Furnace_62180223076.html?spm=a2700.7724857.normal_offer.d_title.f9817524mgz5Sq (accessed 3 January 2023).
68. Federal reserve economic data, Federal Reserve Bank of St. Louis, Producer price index by industry: ready-mix concrete manufacturing: ready-mix concrete for west census region, St. Louis, MO. Retrieved from: https://fred.stlouisfed.org/series/PCU327320327320D (accessed 3 January 2023).